2024 IEEE International Conference on Robotics and Automation (ICRA 2024)
May 13-17, 2024. Yokohama, Japan

Force Estimation at the Bionic Soft Arm's Tool-center-point during the Interaction with the Environment

Samuel Pilch[1], Daniel Klug[2] and Oliver Sawodny[3]

***Abstract*— Soft continuum robots enable new application areas in contrast to standard rigid robots, such as interaction with a varying environment. Due to their compliant continuous structure, they are inherently safe and adaptive to environmental conditions. In this paper, the interaction with the environment is performed at the tool-center-point of a soft continuum manipulator and is realized by a hybrid force-position control. For this, a force estimation model is derived to substitute the force sensor at the tool-center-point. The force estimation is probabilistic and relies on normal distributions considering model parameters and deviations from model identification of the soft continuum robot. It also provides a qualitative measure for the contact estimation. This paper first presents the probabilistic force estimation model and then shows the hybrid force-position control using the presented model. From the results, it is concluded that force sensing is replaceable for the environment interaction.**

I. INTRODUCTION

Soft continuum robots are more suitable for interacting with the environment than traditional rigid robots. They offer an inherent safety towards objects or humans in case of collisions. Because of their continuous structure and the redundancy that comes with it, they can adapt to unstructured, varying environments by bending, twisting or lengthening. This makes them versatile. Moreover, their movements are dexterous that make interactions gentle and thus natural.

In the literature, the interaction with the environment of a soft continuum manipulator is often implemented by Cartesian stiffness or impedance control [1]. Cartesian stiffness control aims to achieve a low stiffness of the manipulator at the contact point. This can be implemented either actively by feedback or passively by changing the manipulator's properties. Cartesian stiffness control is mainly used for small continuum manipulators with a few segments [2], [3]. In impedance control [4], the interaction is modeled as a power exchange between the manipulator and the environment, which is described by a mass-spring-damper system. Impedance control systems, on the other hand, are generally used for small [5], [6] and large soft continuum manipulators [7], [8] with multiple segments.

*This work was supported by German Research Foundation (Deutsche Forschungsgemeinschaft, DFG) under grant no. SA 847/20-2.

[1]Samuel Pilch is a Research Assistant at the Institute for System Dynamics, University of Stuttgart, Waldburgstraße 19, 70563 Stuttgart, Germany samuel.pilch@isys.uni-stuttgart.de

[2]Daniel Klug (né Müller) is a PhD engineer at Qest Antenna Technology GmbH in the Research and Development Department, Max-Eyth-Straße 38, 71088 Holzgerlingen, Germany daniel.klug@qest.de

[3]Oliver Sawodny is a Professor at the Institute for System Dynamics, University of Stuttgart, Waldburgstraße 19, 70563 Stuttgart, Germany sawodny@isys.uni-stuttgart.de

If force sensors are used, force controllers are advantageous because the measured force at the tool-center-point is fed back in the control loop. Especially in the field of minimally invasive surgery, force control has been heavily researched [9], [10], [11], [12], [13], [14], [15]. However, these applications are limited to small soft continuum manipulators.

Hybrid force-position control [16] uses decoupled position as well as force control loops, so that the position can be controlled along unconstrained directions and the force along constrained directions. Bajo et al. [9] presents an active force control system in which a hybrid force-position control is successfully applied to a continuum manipulator with force sensing. A hybrid force-position control combined with model-free control, where the Jacobian is learned in real-time and safely adapts to ambient environmental conditions in a safe manner, is presented by Yip et al. [17]. Müller et al. [15] applies successfully a decoupled hybrid force-position control to a soft continuum manipulator using a disturbance observer. However, in this case the force sensor replaces the gripper at the tool-center-point, so, grasping and manipulating objects is not possible.

This paper presents a tool-center-point force estimation model which replaces the force sensing in the hybrid force-position control loop from Müller et al. [15]. This allows the gripper to be designed independently of a sensor at the tool-center-point as well as saving on the force sensor. A hybrid force-position control without force sensing has already been successfully implemented on rigid articulated manipulators [18], [19], [20], [21]. For soft continuum ma-

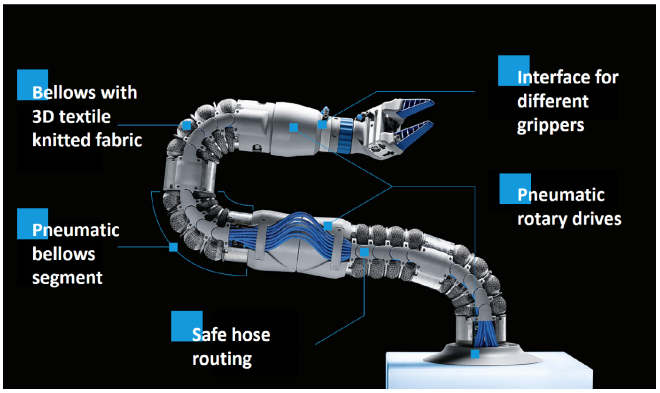

Fig. 1. Bionic soft arm, source: Festo SE & Co. KG. The 1.05 m long soft continuum manipulator is actuated pneumatically by three rotary drives and four bellows segments.

nipulators, this is only applied for small ones with negligible masses [22]. Sadati et al. [23] applies a hybrid force-position control without a force sensor at the tool-center-point of a large soft continuum robot but uses a force sensor in the base of the soft continuum robot.

To the best of our knowledge, a hybrid force-position control using a force estimation model has not yet been applied to soft continuum robots with non-negligible masses and inertias. The paper is structured as follows. The setup of the soft continuum manipulator is introduced in chapter 2. In chapter 3, the force estimation model at the tool-center-point of the soft continuum manipulator is presented. In chapter 4, the force estimation model is validated independently and the hybrid force-position control adapted with. Finally, the validation results are discussed in chapter 5 and in chapter 6, a conclusion of this paper is given.

II. SETUP

A force estimation model is derived replacing the force measurement feedback in the hybrid force-position control loop from Müller et al. [15]. The adapted hybrid force-position control used for interaction with the environment is applied to the bionic soft arm (Fig. 1), which is also used for validation in Müller et al. [15]. The bionic soft arm is a soft continuum manipulator actuated pneumatically by three rotary drives and four bellows segments according to Fig. 2. The kinematics of the bionic soft arm are described by $\boldsymbol{q} \in \mathbb{R}^7$ (Fig. 2) containing the rotation angles of the rotary drives and the bending angles of the bellows segments. The kinetics of the bionic soft arm are described by the equation of motion.

$$\boldsymbol{M}(\boldsymbol{q})\ddot{\boldsymbol{q}} + \boldsymbol{C}(\boldsymbol{q},\dot{\boldsymbol{q}})\dot{\boldsymbol{q}} + \boldsymbol{N}(\boldsymbol{q}) = \boldsymbol{\tau}_{\mathrm{ext}} + \boldsymbol{\tau}_{\mathrm{fric}} + \boldsymbol{\tau}_{\mathrm{act}}, \quad (1)$$

where $\boldsymbol{M}(\boldsymbol{q})$ is the mass matrix, $\boldsymbol{C}(\boldsymbol{q},\dot{\boldsymbol{q}})\dot{\boldsymbol{q}}$ is the vector of Coriolis and centrifugal terms and $\boldsymbol{N}(\boldsymbol{q})$ is the vector of gravitational terms [15]. The right side of the equation contains the external torque $\boldsymbol{\tau}_{\mathrm{ext}}$, the friction torque $\boldsymbol{\tau}_{\mathrm{fric}}$ and the actuator torque $\boldsymbol{\tau}_{\mathrm{act}}$.

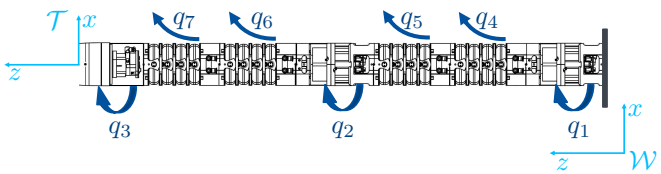

Fig. 2. Kinematics of the bionic soft arm, where q_1, q_2, q_3 are the rotation angles of the rotary drives and q_4, q_5, q_6, q_7 are the bending angles of the bellows segments. $\mathcal{W}$ is the right-handed world coordinate system and $\mathcal{T}$ is the right-handed coordinate system of the tool-center-point.

III. FORCE ESTIMATION MODEL

For the hybrid force-position control without force sensing, an estimation of the external force at the tool-center-point $\hat{\boldsymbol{F}}_{\mathrm{ext}}^{\mathcal{T}} \in \mathbb{R}^3$ is required. This is derived in the following.

The related external torque vector $\boldsymbol{\tau}_{\mathrm{ext}}$ is computed by rearranging (1). Due to inferior measurement of $\boldsymbol{q}$ the derivatives of it are noisy. Moreover, slow movements of the tool-center-point in contact situations are considered, thus $\dot{\boldsymbol{q}}$ and $\ddot{\boldsymbol{q}}$ are neglected. Therefore, the dynamics of the bionic soft arm are neglected leading to the following equation:

$$\hat{\boldsymbol{\tau}}_{\mathrm{ext}} = \boldsymbol{N}(\boldsymbol{q}) - \boldsymbol{\tau}_{\mathrm{act}}, \quad (2)$$

where $\hat{\boldsymbol{\tau}}_{\mathrm{ext}}$ is the estimated external torque. The estimated external torque $\hat{\boldsymbol{\tau}}_{\mathrm{ext}}$ is transformed into a cartesian coordinate system with its origin in the tool-center-point by the mapping $\boldsymbol{\Gamma}(\boldsymbol{q}) = \boldsymbol{J}^{\intercal}(\boldsymbol{q})$. $\boldsymbol{J}^{\intercal}(\boldsymbol{q})$ is the transposed Jacobian of $\boldsymbol{q}$ at the tool-center-point. The equation holds

$$\hat{\boldsymbol{\tau}}_{\mathrm{ext}} = \boldsymbol{\Gamma}(\boldsymbol{q})\hat{\boldsymbol{F}}_{\mathrm{ext}}^{\mathcal{T}} \quad (3)$$

according to Siciliano et al. [24]. Using the regularized pseudoinverse of the mapping, $\boldsymbol{\Gamma}_{\mathrm{r}}(\boldsymbol{q})$, the estimated external force at the tool-center-point is computed by

$$\begin{aligned} \boldsymbol{\Gamma}_{\mathrm{r}}^{+}(\boldsymbol{q}) &= \left(\boldsymbol{\Gamma}^{\intercal}(\boldsymbol{q})\boldsymbol{\Gamma}(\boldsymbol{q}) + \varepsilon \boldsymbol{I}\right)^{-1}\boldsymbol{\Gamma}^{\intercal}(\boldsymbol{q}), \\ \hat{\boldsymbol{F}}_{\mathrm{ext}}^{\mathcal{T}} &= \boldsymbol{\Gamma}_{\mathrm{r}}^{+}(\boldsymbol{q})\hat{\boldsymbol{\tau}}_{\mathrm{ext}}, \end{aligned} \quad (4)$$

where $\varepsilon < 10^{-7}$. In the static case, i.e., constant actuator pressures without external tool-center-point forces, the estimated external torque does not vanish, $\hat{\boldsymbol{\tau}}_{\mathrm{ext}} \neq \boldsymbol{0}$. This is due to static friction as well as model deviations. In particular, it is unclear whether static friction supports or opposes the actuator torque $\boldsymbol{\tau}_{\mathrm{act}}$.

The pressure-dependent static friction values are described by $\boldsymbol{\delta}_{\mathrm{fric}}(\boldsymbol{p}) \in \mathbb{R}^7$. From model identification follows that the model deviations of the bellows for the static case are up to $0.9\,\mathrm{N\,m}$. The static deviations of the rotary actuators are vanishingly small. Thus, the maximal deviations of the static model result in

$$\boldsymbol{\delta}_{\mathrm{model,stat}} = \begin{bmatrix} 0\,\mathrm{N\,m} \\ 0\,\mathrm{N\,m} \\ 0\,\mathrm{N\,m} \\ 0.9\,\mathrm{N\,m} \\ 0.9\,\mathrm{N\,m} \\ 0.9\,\mathrm{N\,m} \\ 0.9\,\mathrm{N\,m} \end{bmatrix}. \quad (5)$$

A measure of the maximal dynamic model deviations is obtained during movements from the estimated torque of the disturbance observer [25] used in the hybrid force-position control loop [15] to

$$\boldsymbol{\delta}_{\mathrm{model,dyn}} = \begin{bmatrix} 2\,\mathrm{N\,m} \\ 1.5\,\mathrm{N\,m} \\ 0.3\,\mathrm{N\,m} \\ 2\,\mathrm{N\,m} \\ 2\,\mathrm{N\,m} \\ 2\,\mathrm{N\,m} \\ 2\,\mathrm{N\,m} \end{bmatrix}. \quad (6)$$

The lack of knowledge about the current magnitude and direction of action of the static friction as well as the static and dynamic model deviations is expressed by the normal distributions $\mathcal{T}_{\mathrm{stat}}$ and $\mathcal{T}_{\mathrm{dyn}}$

$$\begin{aligned} \mathcal{T}_{\mathrm{stat}} &\sim \mathcal{N}\left(\hat{\boldsymbol{\tau}}_{\mathrm{ext}}, \boldsymbol{\Sigma}_{\mathrm{stat}}\right), \\ \mathcal{T}_{\mathrm{dyn}} &\sim \mathcal{N}\left(\hat{\boldsymbol{\tau}}_{\mathrm{ext}}, \boldsymbol{\Sigma}_{\mathrm{dyn}}\right), \end{aligned} \quad (7)$$

where $\hat{\boldsymbol{\tau}}_{\mathrm{ext}}$ is the expected value and $\boldsymbol{\Sigma}_{\mathrm{stat}}$ as well as $\boldsymbol{\Sigma}_{\mathrm{dyn}}$ are the covariance matrices. It is assumed that friction and model deviations of the individual joints are independent of each other. Furthermore, it is assumed that the maximal observed deviations are three times the standard deviation, about $99.73\,\%$, of the normally distributed deviations. Thus, the covariance matrices result in

$$\begin{aligned}\boldsymbol{\Sigma}_{\mathrm{stat}}(\boldsymbol{p}) &= \operatorname{diag}\left(\left(\frac{1}{3}\left(\boldsymbol{\delta}_{\mathrm{fric}}(\boldsymbol{p}) + \boldsymbol{\delta}_{\mathrm{model,stat}}\right)\right)^{\circ 2}\right),\\ \boldsymbol{\Sigma}_{\mathrm{dyn}}(\boldsymbol{p}) &= \operatorname{diag}\left(\left(\frac{1}{3}\left(\boldsymbol{\delta}_{\mathrm{fric}}(\boldsymbol{p}) + \boldsymbol{\delta}_{\mathrm{model,dyn}}\right)\right)^{\circ 2}\right),\end{aligned} \tag{8}$$

where '$\circ 2$' represents the element-wise squaring of the vectors and the operator diag returns a square diagonal matrix with the elements of its argument on the main diagonal. Since a linear combination of normal distributions results in a normal distribution again, the estimated external force at the tool-center-point is described as a random variable

$$\mathcal{F}^{\mathcal{T}}_{\mathrm{ext},\star} \sim \mathcal{N}\left(\hat{\boldsymbol{F}}^{\mathcal{T}}_{\mathrm{ext}}, \boldsymbol{\Gamma}^{+}_{\mathrm{r}}(\boldsymbol{q})\boldsymbol{\Sigma}_{\star}\boldsymbol{\Gamma}^{+\intercal}_{\mathrm{r}}(\boldsymbol{q})\right), \tag{9}$$

where $\star \in \{\mathrm{stat}, \mathrm{dyn}\}$ to distinguish between the static and the dynamic force estimation at the tool-center-point.

In the following, a measure is derived which indicates a probability that a contact is present at the tool-center-point of the bionic soft arm. For this purpose, the normed estimated direction of the external force at the tool-center-point is described as

$$\boldsymbol{d} = \frac{1}{\left\|\hat{\boldsymbol{F}}^{\mathcal{T}}_{\mathrm{ext}}\right\|}\hat{\boldsymbol{F}}^{\mathcal{T}}_{\mathrm{ext}}. \tag{10}$$

If the random variable $\mathcal{F}^{\mathcal{T}}_{\mathrm{ext},\star}$ is projected along this direction, the normal distribution of the estimated external force at the tool-center-point is obtained with

$$\mathcal{F}^{\mathcal{T}}_{\mathrm{C},\star} \sim \mathcal{N}(\underbrace{\boldsymbol{d}^{\intercal}\hat{\boldsymbol{F}}^{\mathcal{T}}_{\mathrm{ext}}}_{\mu_{\mathrm{C}}}, \underbrace{\boldsymbol{d}^{\intercal}\boldsymbol{\Gamma}^{+}_{\mathrm{r}}(\boldsymbol{q})\boldsymbol{\Sigma}_{\star}(\boldsymbol{p})\boldsymbol{\Gamma}^{+\intercal}_{\mathrm{r}}(\boldsymbol{q})\boldsymbol{d}}_{\sigma^2_{\mathrm{C},\star}}). \tag{11}$$

Hence, the expected value of the normal distribution of the estimated external force at the tool-center-point is

$$\mu_{\mathrm{C}} = \left\|\hat{\boldsymbol{F}}^{\mathcal{T}}_{\mathrm{ext}}\right\|. \tag{12}$$

Thus, $\mu_{\mathrm{C}} \geq 0$ is always satisfied. Further, it should be noted that due to the symmetry of the normally distributed $\mathcal{F}^{\mathcal{T}}_{\mathrm{C},\star}$ negative values of $\mathcal{F}^{\mathcal{T}}_{\mathrm{C},\star}$ are possible. In particular, for $\mu_{\mathrm{C}} = 0$, the random variable $\mathcal{F}^{\mathcal{T}}_{\mathrm{C},\star}$ is negative with a probability of $50\,\%$. These negative values are not physically meaningful, since the interaction of the tool-center-point with the environment is always measured by a positive external force. So, it is assumed that $\mathcal{F}^{\mathcal{T}}_{\mathrm{C},\star} \leq 0$ corresponds to the contactless case, hence, the probability that no external force at the tool-center-point is applied results in

$$\begin{aligned}\neg P_{\mathrm{C},\star} &= 2P\left(\mathcal{F}^{\mathcal{T}}_{\mathrm{C},\star} \leq 0\right)\\ &= \int_{-\infty}^{0} \mathcal{N}\left(x \mid \mu_{\mathrm{C}}, \sigma^2_{\mathrm{C},\star}\right) \mathrm{d}x.\end{aligned} \tag{13}$$

The complementary event that an external force is applied is described by

$$P_{\mathrm{C},\star} = 1 - \neg P_{\mathrm{C},\star}. \tag{14}$$

IV. VALIDATION

A. Experimental Validation of the Force Estimation at the Tool-center-point

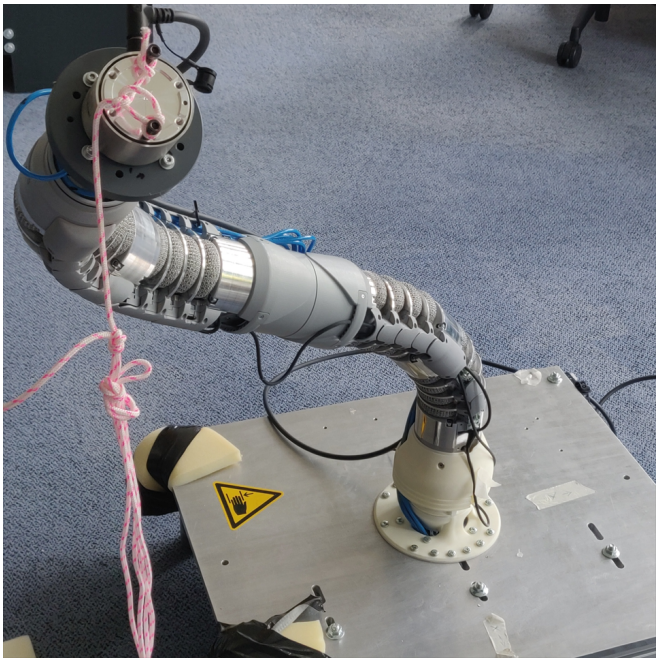

Fig. 3. The experimental setup for estimating an external force. An external force is applied to the bionic soft arm by the nylon thread at the tool-center-point. This force causes movement in the joints. At the same time, the position control tries to maintain the initial position.

In the following, the force estimation at the tool-center-point is validated experimentally. The experimental setup is shown in Fig. 3. A punctiform external force is applied to the bionic soft arm at the tool-center-point by pulling the nylon thread. The applied external force, which causes the bionic soft arm to move, is measured by the force sensor at the tool-center-point. During the experiment, the bionic soft arm is supposed to hold the shown initial position by the position controller [15]. Fig. 4 shows the measured $\left\|\boldsymbol{F}^{\mathcal{T}}_{\mathrm{ext}}\right\|$ and estimated external force $\left\|\hat{\boldsymbol{F}}^{\mathcal{T}}_{\mathrm{ext}}\right\|$ along with its angular error

$$\begin{aligned}e_{\sphericalangle} &= \operatorname{angle}\left(\hat{\boldsymbol{F}}^{\mathcal{T}}_{\mathrm{ext}}, \boldsymbol{F}^{\mathcal{T}}_{\mathrm{ext}}\right)\\ &= \cos^{-1}\left(\frac{\hat{\boldsymbol{F}}^{\mathcal{T}\intercal}_{\mathrm{ext}}\boldsymbol{F}^{\mathcal{T}}_{\mathrm{ext}}}{\left\|\hat{\boldsymbol{F}}^{\mathcal{T}}_{\mathrm{ext}}\right\|\left\|\boldsymbol{F}^{\mathcal{T}}_{\mathrm{ext}}\right\|}\right).\end{aligned} \tag{15}$$

Fig. 4 also shows the estimated probability $P_{\mathrm{C,dyn}}$ that an external force is applied causing the bionic soft arm to move. In Fig. 4, it can be seen that the confidence interval of $\pm 2\sigma_{\mathrm{C,dyn}}$, which is chosen instead of $\pm 3\sigma_{\mathrm{C,dyn}}$ for a better clarity, is not constant since the accuracy of the force estimation depends on the direction of the force and the joint positions of the bionic soft arm $\boldsymbol{q}$. Typically, a

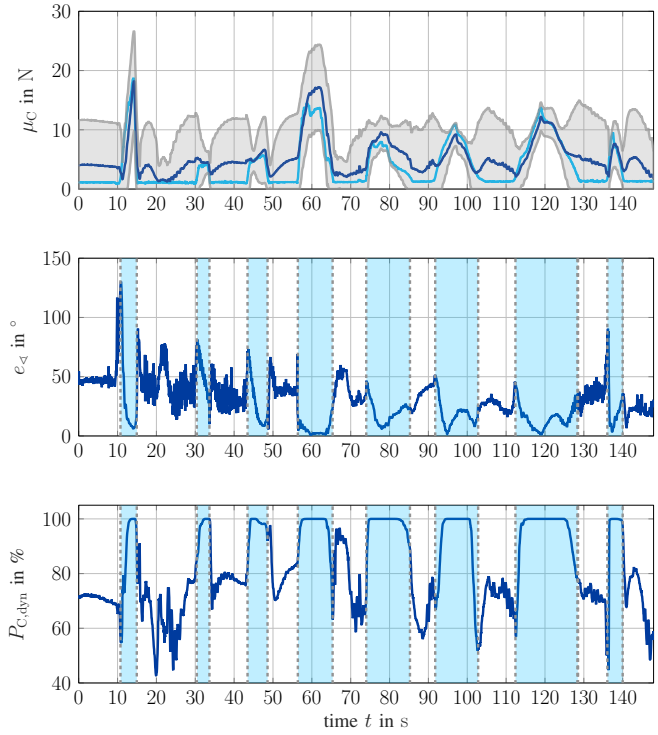

Fig. 4. Contact detection and force estimation. In the top measurement plot, μ_C is shown in (—) and $\left\|\boldsymbol{F}_{ext}^{\mathcal{T}}\right\|$ is shown in (—). The light gray colored area shows $\pm 2\sigma_{C,dyn}$, being about 95.5 % of the confidence interval of $\mathcal{F}_{C,\star}^{\mathcal{T}}$. The middle measurement plot shows the deviation of the force direction $e_\sphericalangle$ and the bottom measurement plot shows the estimated probability of contact $P_{C,dyn}$. In the middle and bottom measurement plots, the blue colored sections show when $\left\|\boldsymbol{F}_{ext}^{\mathcal{T}}\right\| \geq 2$ N is satisfied and thus an external force acts.

large applied force can be reconstructed better, as the given model deviations are less important. During a contact, the average angular error $e_\sphericalangle$ is about 20° and the average error between estimated and measured force is 1.68 N. Over the entire period, the error of force estimation is 2.06 N. The probability of contact $P_{C,dyn}$ is greater than 99 % during each contact situation, i.e., applying external forces.

B. Experimental Validation of the Hybrid Force-position Control with Force Estimation

In contrast to the experimental validation of the force estimation at the tool-center-point, the direction of the external force at the tool-center-point is already known for hybrid force-position control. For the hybrid force-position control with force estimation, the already presented control scheme from Müller et al. [15] is used. Further, if no desired motion is specified during contact, the model deviations are reduced to the static case. Thus, the normal distribution of the estimated force at the tool-center-point in $z^{\mathcal{T}}$-direction, being the normal direction of the tool-center-point plane (Fig. 2), is given by

$$\mathcal{F}_{ext,z,stat}^{\mathcal{T}} \sim \mathcal{N}\left(\mu_{C,ctrl}, \sigma_{C,ctrl}^2\right), \tag{16}$$

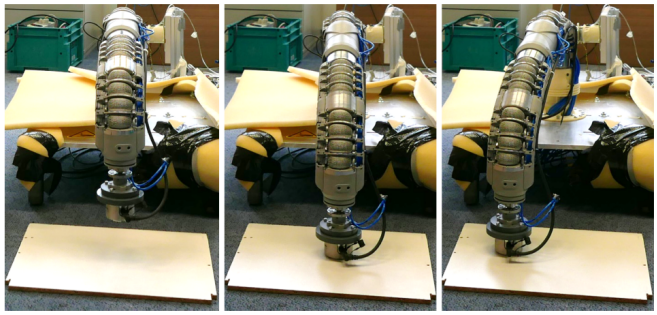

Fig. 5. The experimental procedure of the force experiments. In the left figure, the tool-center-point of the bionic soft arm moves in the direction of the object. Here, the position control is active. In the middle figure, the contact between the tool-center-point and the object happens, thus, the hybrid force-position control is activated. In the right picture hybrid force-position control is active applying forces and holding position.

with

$$\mu_{C,ctrl} = \begin{bmatrix} 0 & 0 & 1 \end{bmatrix} \hat{\boldsymbol{F}}_{ext}^{\mathcal{T}},$$

$$\sigma_{C,ctrl}^2 = \begin{bmatrix} 0 & 0 & 1 \end{bmatrix} \boldsymbol{\Gamma}_r^{+}(\boldsymbol{q}) \boldsymbol{\Sigma}_{stat}(\boldsymbol{p}) \boldsymbol{\Gamma}_r^{+\intercal}(\boldsymbol{q}) \begin{bmatrix} 0 \\ 0 \\ 1 \end{bmatrix}. \tag{17}$$

Since the sign of the expected contact force is known, i.e., the force is negative for push, the probability of the contact between the tool-center-point and the environment is given by

$$P_{C,ctrl} = \int_{-\infty}^{0} \mathcal{N}\left(x \mid \mu_{C,ctrl}, \sigma_{C,ctrl}^2\right) \mathrm{d}x. \tag{18}$$

In contrast to the Müller et al. [15], who use a force sensor, here, a contact is detected as soon as $P_{C,ctrl} \geq 99.73\,\%$, which corresponds to a confidence interval of $\pm 3\sigma_{C,ctrl}$. Subsequently, hybrid force-position control is activated, but $\mu_{C,ctrl}$ is fed back instead of the sensor signal. The validation procedure of the hybrid force-position control is shown in Fig. 5.

Fig. 6 shows the measurements of the validation procedure. Here, the $z^{\mathcal{W}}$-axis is parallel to the $z^{\mathcal{T}}$-axis. In comparison to the validation procedure with a force sensor (Fig. 7), the position control is switched later to the hybrid force-position control. This can be seen in the desired trajectory of the $z^{\mathcal{W}}$-coordinate reaching -0.2 m in contrast to -0.18 m. This leads to a time delay of about 2.3 s before the hybrid force-position control is activated.

Fig. 8 shows the force trajectory sequence of the validation procedure without the usage of a force sensor. The top measurement plot indicates that the measured force $F_{ext,z}^{\mathcal{T}}$ is almost always within the 68.27 %–confidence interval with $\mu_{C,ctrl} \pm \sigma_{C,ctrl}$, which is chosen instead of $\mu_{C,ctrl} \pm 3\sigma_{C,ctrl}$ for a better illustration. The error between the estimated and the measured force is consistently below 2 N and is on average 0.49 N. Especially large forces are estimated more reliably, due to the constant model deviations in the almost constant configuration (Fig. 5). Throughout the force

trajectory, the probability for a contact force $P_{\mathrm{C,ctrl}}$ remains above 98.5 %.

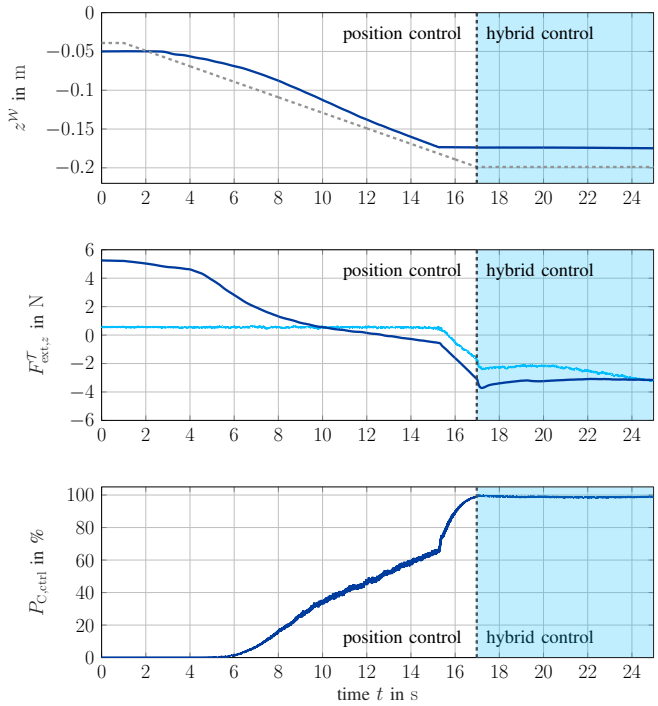

Fig. 6. The validation procedure of the force control with force estimation. In the top measurement plot the $z^{\mathcal{W}}$-position of the tool-center-point of the bionic soft arm is shown. The reference is colored in (– –) and the measured value in (—). The middle measurement plot shows the estimated force $\mu_{\mathrm{C,ctrl}}$ in (—) and the force $F^{\mathcal{T}}_{\mathrm{ext},z}$ measured at the tool-center-point after filtering in (—). The bottom measurement plot illustrates the probability $P_{\mathrm{C,ctrl}}$ in (—), indicating that an external force is applied. The time period when the hybrid force-position control is active is colored in light blue. The hybrid force-position control is turned on as soon as $P_{\mathrm{C,ctrl}} \geq 99.73\,\%$.

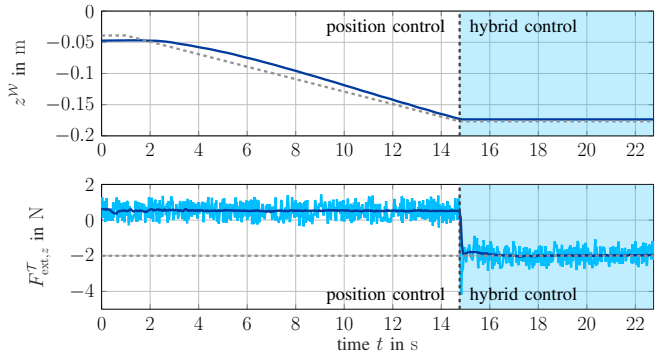

Fig. 7. The validation procedure of the force control with a force sensor at the tool-center-point. The top measurement plot shows the course of the $z^{\mathcal{W}}$-position of the tool-center-point of the bionic soft arm (—) and its desired position in (– –). The bottom measurement plot shows the force curve of the sensor $F^{\mathcal{T}}_{\mathrm{ext,z}}$ in (—). The filtered sensor signal is shown in (—). The force reference is plotted in (– –). The area where the hybrid force-position control is activated is colored light blue.

V. DISCUSSION

First and foremost, the estimation of the external force at the tool-center-point $\boldsymbol{F}^{\mathcal{T}}_{\mathrm{ext}}$ is based on the torque estimations of the bionic soft arm $\hat{\boldsymbol{\tau}}_{\mathrm{ext}}$, which neglect dynamics according to (2). So, the static case is considered. This is valid for the experimental validation of the hybrid force-position control with force estimation, as the motion is neglectable, but has drawbacks for the experimental validation of the force estimation at the tool-center-point, as motions are occurring here, which are considered by the dynamic covariance matrix for dynamical model deviations $\boldsymbol{\Sigma}_{\mathrm{dyn}}$. Fig. 4 shows difficulties in estimating the external force directions, especially in the beginning of the contact when movement of the bionic soft arm occurs. This can be explained by the dynamic model deviations and the slow dynamics of the disturbance observer. However, the estimation of the applied external force $\left\|\hat{\boldsymbol{F}}^{\mathcal{T}}_{\mathrm{ext}}\right\|$ and the related probability $P_{\mathrm{C,dyn}}$ works well, since the estimated external force is almost always in the confidential interval and the contact detection is reliable and quick enough. This result is confirmed by the experimental validation of the hybrid force-position control with force estimation as shown in Fig. 6 and Fig. 8. Compared to the hybrid force-position control with force sensing (Fig. 7), there is a time delay for contact detection of about 2.3 s. This is because external forces of larger than 2 N are required for contact detection, i.e. $P_{\mathrm{C,ctrl}} \geq 99.73\,\%$, due to model deviations of the bionic

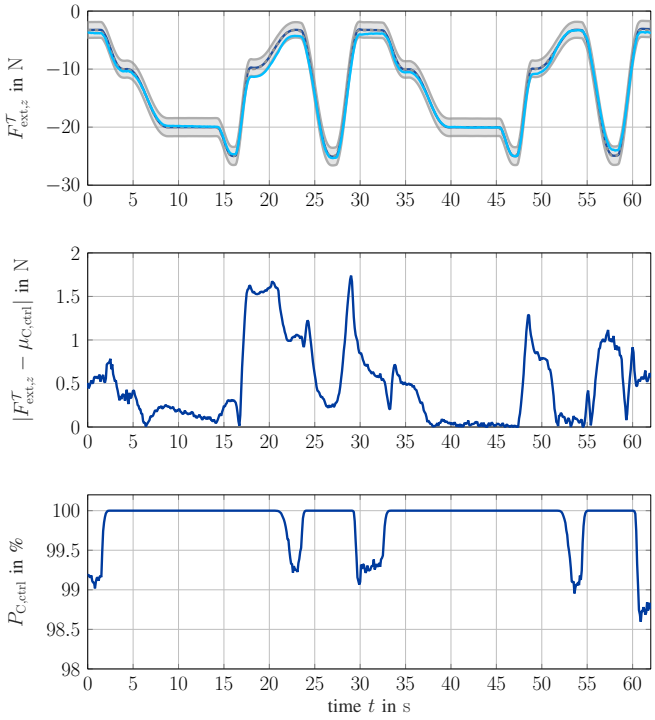

Fig. 8. The force trajectory sequence is shown. In the top measurement plot, (—) shows the estimated external force $\mu_{\mathrm{C,ctrl}}$ and (—) shows the force $F^{\mathcal{T}}_{\mathrm{ext},z}$ measured at the tool-center-point by the force sensor. The gray colored area shows the 68.27 %–confidence interval with $\mu_{\mathrm{C,ctrl}} \pm \sigma_{\mathrm{C,ctrl}}$. The desired reference force is shown in (– –). The middle measurement plot shows the control error of the force. The bottom measurement plot shows the probability $P_{\mathrm{C,ctrl}}$ of a contact force. The bionic soft arm is in contact with the environment for the complete duration of the experiment. The corresponding pose of the manipulator is shown in the right subfigure of Fig. 3.

soft arm. However, regarding the application, the time delay is small. In total, the detection of contact at the tool-center-point works reliably.

Overall, the hybrid force-position control with force estimation works reliably, such that the force sensor can be removed if the external forces to be estimated are large compared to the model deviations.

VI. CONCLUSIONS

In this paper, a probabilistic force estimation model of the bionic soft arm is derived. It consists of the static $\mathcal{F}^{\mathcal{T}}_{\mathrm{ext,stat}}$ and the dynamic model $\mathcal{F}^{\mathcal{T}}_{\mathrm{ext,dyn}}$ for estimating the external force at the tool-center-point. They are based on normal distributions considering model parameters and deviations from model identification of the bionic soft arm. Based on this, a qualitative measure for contact estimation $P_{\mathrm{C},\star}, \star \in \{\mathrm{stat}, \mathrm{dyn}\}$ is derived which is also part of the force estimation model. The force estimation model is validated successfully in experiments.

The interaction with the environment is performed by the hybrid force-position control [15] using the derived and validated force estimation model instead of force sensing. For this, the estimated force is mapped onto the normal direction of the tool-center-point plane. Based on the contact estimation $P_{\mathrm{C},\star}$, the contact detection is defined as $P_{\mathrm{C,ctrl}} \geq 99.73\,\%$, which corresponds to a probability of larger or equal than a confidence interval of ± 3 standard deviations. The adapted hybrid force-position control is able to detect contacts reliably in experiments for contact forces larger than $2\,\mathrm{N}$. In this case, the force sensor can be substituted.

Future work may include the implementation of a sensorless gripper instead of a force sensor at the tool-center-point of the bionic soft arm. Moreover, the contact detection can be extended to any position at the bionic soft arm considering unexpected contacts as well.

ACKNOWLEDGMENT

This work was supported by German Research Foundation (Deutsche Forschungsgemeinschaft, DFG) under grant no. SA 847/20-2.

REFERENCES

[1] C. Della Santina, C. Duriez, and D. Rus, "Model-Based Control of Soft Robots: A Survey of the State of the Art and Open Challenges," *IEEE Control Systems Magazine*, vol. 43, pp. 30–65, June 2023.

[2] M. Mahvash and P. E. Dupont, "Stiffness control of a continuum manipulator in contact with a soft environment," in *2010 IEEE/RSJ International Conference on Intelligent Robots and Systems*, pp. 863–870, Oct. 2010. ISSN: 2153-0866.

[3] M. Mahvash and P. E. Dupont, "Stiffness Control of Surgical Continuum Manipulators," *IEEE Transactions on Robotics*, vol. 27, pp. 334–345, Apr. 2011.

[4] N. Hogan, "Impedance Control: An Approach to Manipulation," in *1984 American Control Conference*, pp. 304–313, June 1984.

[5] C. Della Santina, R. K. Katzschmann, A. Biechi, and D. Rus, "Dynamic control of soft robots interacting with the environment," in *2018 IEEE International Conference on Soft Robotics (RoboSoft)*, pp. 46–53, Apr. 2018.

[6] C. Della Santina, R. K. Katzschmann, A. Bicchi, and D. Rus, "Model-based dynamic feedback control of a planar soft robot: trajectory tracking and interaction with the environment," *The International Journal of Robotics Research*, vol. 39, no. 4, pp. 490–513, 2020.

[7] L. Toscano, V. Falkenhahn, A. Hildebrandt, F. Braghin, and O. Sawodny, "Configuration space impedance control for continuum manipulators," in *2015 6th International Conference on Automation, Robotics and Applications (ICARA)*, pp. 597–602, Feb. 2015.

[8] G. He, Y. Fan, T. Su, L. Zhao, and Q. Zhao, "Variable Impedance Control of Cable Actuated Continuum Manipulators," *International Journal of Control, Automation and Systems*, vol. 18, pp. 1839–1852, July 2020.

[9] A. Bajo and N. Simaan, "Hybrid motion/force control of multi-backbone continuum robots," *The International Journal of Robotics Research*, vol. 35, pp. 422–434, Apr. 2016.

[10] R. E. Goldman, A. Bajo, and N. Simaan, "Compliant motion control for continuum robots with intrinsic actuation sensing," in *2011 IEEE International Conference on Robotics and Automation*, pp. 1126–1132, May 2011. ISSN: 1050-4729.

[11] S. M. Mustaza, C. M. Saaj, F. J. Comin, W. A. Albukhanajer, D. Mahdi, and C. Lekakou, "Stiffness control for soft surgical manipulators," *International Journal of Humanoid Robotics*, vol. 15, no. 05, p. 1850021, 2018.

[12] S. H. Sadati, Y. Noh, S. Elnaz Naghibi, K. Althoefer, and T. Nanayakkara, "Stiffness control of soft robotic manipulator for minimally invasive surgery (mis) using scale jamming," in *Intelligent Robotics and Applications: 9th International Conference, ICIRA 2015, Portsmouth, UK, August 2427, 2015, Proceedings, Part III*, pp. 141–151, Springer, 2015.

[13] M. K. Soltani, S. Khanmohammadi, F. Ghalichi, and F. Janabi-Sharifi, "A soft robotics nonlinear hybrid position/force control for tendon driven catheters," *International Journal of Control, Automation and Systems*, vol. 15, pp. 54–63, 2017.

[14] Z. Zhang, J. Dequidt, J. Back, H. Liu, and C. Duriez, "Motion control of cable-driven continuum catheter robot through contacts," *IEEE Robotics and Automation Letters*, vol. 4, no. 2, pp. 1852–1859, 2019.

[15] D. Müller, C. Veil, and O. Sawodny, "Hybrid force/position control for quasi continuum manipulators," *at-Automatisierungstechnik*, vol. 68, no. 10, pp. 854–862, 2020.

[16] M. H. Raibert and J. J. Craig, "Hybrid position/force control of manipulators," 1981.

[17] M. C. Yip and D. B. Camarillo, "Model-less hybrid position/force control: a minimalist approach for continuum manipulators in unknown, constrained environments," *IEEE Robotics and Automation Letters*, vol. 1, no. 2, pp. 844–851, 2016.

[18] A. Wahrburg, B. Matthias, and H. Ding, "Cartesian Contact Force Estimation for Robotic Manipulators - A Fault Isolation Perspective," *IFAC-PapersOnLine*, vol. 48, pp. 1232–1237, Jan. 2015.

[19] A. Wahrburg, E. Morara, G. Cesari, B. Matthias, and H. Ding, "Cartesian contact force estimation for robotic manipulators using Kalman filters and the generalized momentum," in *2015 IEEE International Conference on Automation Science and Engineering (CASE)*, pp. 1230–1235, Aug. 2015. ISSN: 2161-8089.

[20] A. Wahrburg, A. Robertsson, B. Matthias, F. Dai, and H. Ding, "Improving contact force estimation accuracy by optimal redundancy resolution," in *2016 IEEE/RSJ International Conference on Intelligent Robots and Systems (IROS)*, pp. 3735–3741, IEEE, 2016.

[21] E. Magrini, F. Flacco, and A. De Luca, "Estimation of contact forces using a virtual force sensor," in *2014 IEEE/RSJ International Conference on Intelligent Robots and Systems*, pp. 2126–2133, IEEE, 2014.

[22] R. Yasin and N. Simaan, "Joint-level force sensing for indirect hybrid force/position control of continuum robots with friction," *The International Journal of Robotics Research*, vol. 40, no. 4-5, pp. 764–781, 2021.

[23] S. H. Sadati, A. Shiva, N. Herzig, C. D. Rucker, H. Hauser, I. D. Walker, C. Bergeles, K. Althoefer, and T. Nanayakkara, "Stiffness imaging with a continuum appendage: Real-time shape and tip force estimation from base load readings," *IEEE Robotics and Automation Letters*, vol. 5, no. 2, pp. 2824–2831, 2020.

[24] B. Siciliano, O. Khatib, and T. Kröger, *Springer handbook of robotics*, vol. 200. Springer, 2008.

[25] D. Müller, C. Veil, and O. Sawodny, "Disturbance Observer Based Control for Quasi Continuum Manipulators," *IFAC-PapersOnLine*, vol. 53, pp. 9808–9813, Jan. 2020.